Fibrillar Elastomeric Micropatterns Create Tunable Adhesion Even to Rough Surfaces

*Viktoriia Barreau, René Hensel, Nathalie K. Guimard, Animangsu Ghatak, Robert M. McMeeking, and Eduard Arzt**

Biologically inspired, fibrillar dry adhesives continue to attract much attention as they are instrumental for emerging applications and technologies. To date, the adhesion of micropatterned gecko-inspired surfaces has predominantly been tested on stiff, smooth substrates. However, all natural and almost all artificial surfaces have roughnesses on one or more different length scales. In the present approach, micropillar-patterned PDMS surfaces with superior adhesion to glass substrates with different roughnesses are designed and analyzed. The results reveal for the first time adhesive and nonadhesive states depending on the micropillar geometry relative to the surface roughness profile. The data obtained further demonstrate that, in the adhesive regime, fibrillar gecko-inspired adhesive structures can be used with advantage on rough surfaces; this finding may open up new applications in the fields of robotics, biomedicine, and space exploration.

1. Introduction

The gecko is considered to be the most interesting animal among those that have the remarkable ability to reversibly adhere to nearly all kinds of surfaces. The growing number of studies published in this field in the last two decades reflects the interest in elucidating the mechanism behind gecko adhesion. Experimental evidence has suggested that the adhesive ability of geckos can be attributed to van der Waals and capillary forces.[1–5] These forces are maximized by the structure of the gecko toe pad, which is composed of hundreds of thousands of keratinous hairs (called setae). Each hair is about 110 µm long and branches into hundreds of even finer hairs (called spatula) that are about 20 nm thick and 200 nm long. Thus, the gecko relies on hierarchically organized structures consisting of micro- and nanosized hairy features to achieve adhesion to almost any surface.[6–11]

There are several studies that have demonstrated and characterized the adhesion of gecko-inspired micropatterned surfaces on hard, smooth substrates (for reviews see, for instance, refs. [12–19]). However, considering that all natural and almost all artificial surfaces have a roughness on one or more different length scales, little research has been conducted to comprehend and optimize the adhesion of such structures to rough surfaces. Huber et al.[20] are among the few that have performed such studies, which include measurements, by atomic force microscopy (AFM), of the normal adhesion of a single gecko spatula to substrates with different roughnesses. They found that a spatula adapts well to a surface with a low root mean square (RMS) roughness (smaller than 200 nm) and also adheres strongly to substrates with an RMS roughness above 200 nm, but shows a distinct minimum in adhesion at RMS roughness of 200 nm, which is a typical spatula dimension. Recently, Gillies[21] observed a similar dramatic drop of shear resistance for geckos on wavy substrates that exhibited a length scale of amplitudes and wavelengths similar to the lamella length and interlamellar spacing, specifically in the submillimeter range. Persson performed the first theoretical studies on adhesion as a function of the fibrillar architecture and surface roughness.[22,23] He demonstrated that even a relatively small roughness can lead to the disappearance of the adhesion between two surfaces. More recently, studies on the influence of technologically relevant rough surfaces on the adhesion of biomimetic adhesives confirmed that adhesion decreases for rough surfaces when compared to smooth surfaces.[24–30]

Because little is known about the influence of micropillar dimensions on dry adhesion of gecko-mimicking structures on rough substrates, the objective of this study is to systematically

V. Barreau, Dr. R. Hensel, Dr. N. K. Guimard, Prof. A. Ghatak, Prof. R. M. McMeeking, Prof. E. Arzt
INM - Leibniz Institute for New Materials
Campus D2 2 66123, Saarbrücken, Germany
E-mail: eduard.arzt@leibniz-inm.de
V. Barreau, Prof. E. Arzt
Department of Materials Science and Engineering
Saarland University
66123 Saarbrücken, Germany
Prof. A. Ghatak
Department of Chemical Engineering
Indian Institute of Technology
208016 Kanpur, India
Prof. R. M. McMeeking
Materials Department and Department of Mechanical Engineering
University of California
Santa Barbara, CA 93106, USA
Prof. R. M. McMeeking
Engineering School
University of Aberdeen
King's College
Aberdeen AB24 3UE, UK

DOI: 10.1002/adfm.201600652

and quantitatively characterize this effect. Arrays with different micropillar dimensions were generated from polydimethylsiloxane (PDMS) using soft molding techniques. Then, the influence of pillar diameter and height on adhesion to a number of stiff substrates with different roughness was assessed. The goal was to improve the understanding of the role of surface roughness, in comparison to smooth controls.

2. Results

Micropatterned elastomeric PDMS adhesives were produced via a soft molding process from a micropatterned SU-8 photoresist master template (**Figure 1**A). To realize the tone inversion, the PDMS replica generated after the first molding process was in turn used as a template for a second replication step, again by soft molding PDMS. By varying the resist thickness and the mask pattern dimensions, specimens with micropillar structures ranging from 5 to 50 µm in pillar diameter, D, and from 5 to 75 µm in pillar height, H, were fabricated. Figure 1B shows a representative scanning electron micrograph of a micropatterned PDMS specimen. PDMS pillar structures, particularly of small diameters with an aspect ratio, H/D, larger than 4, tended to cluster due to an insufficient bending stiffness. To avoid such artifacts, adhesion measurements were limited to specimens with a maximum aspect ratio of about 3. Figure 1C schematically illustrates the setup for testing adhesion of the fabricated specimens to several rough substrates. The custom-built device consists of the nominally flat, but microrough substrate mounted on the flexure beam and a pivotable stage allowing for specimen manipulation (attachment and detachment) and for the required prealignment. A laser interferometer was used to record beam deflection, which was converted into a force through multiplication by the spring constant of the flexure beam.[31]

Figure 2 depicts the characteristic height–distance profile, obtained using surface contact profilometry, for glass substrates (GS) roughened with sandpaper. The surface roughness parameters are schematically illustrated in Figure 2B and the measured surface roughness values for each substrate are tabulated in Figure 2C. For the substrates GS1 to GS4, the vertical roughness parameter (R_z), which is the mean peak to valley distance increases from 0.7 to 9.7 µm and the lateral spacing parameter (S_m), which is the mean distance of the spacing between successive points as they cross the mean line, increases from 31.7 to 87 µm. Additionally, the mean distance between adjacent peaks (S) slightly decreases from 16.4 to 10.3 µm. The increase of roughness from GS1 to GS4 is also reflected in the Fourier transformed data based on line scans (Figure 2D). The power spectra indicate a random, self-affine roughness of the substrates upon sandpaper roughening due to the continuous decrease of the square amplitude with increasing wave numbers.[32]

The adhesion measurements were performed by pressing the micropatterned adhesives onto the substrates in the normal direction with various preloads of 10, 25, and 40 mN. The results for the rough substrates GS1 and GS3 and the smooth control are shown as double-logarithmic plots in **Figure 3**A. Adhesion is seen to decrease strongly with increasing roughness, which is in agreement with earlier studies with unpatterned elastomeric specimens.[33–35] In addition, the pull-off stress for the smooth substrate was found to be preload independent in line with our earlier studies,[36] whereas a strong influence of preload was observed for the rough substrates. This finding is significant and will be discussed in more detail in the next section.

In Figure 3A, it is further shown that the pull-off stress increases for smaller pillar diameters in the case of the smooth substrate. It is now accepted that for a patterned adhesive surface, like that of the gecko foot, a "contact splitting" mechanism significantly enhances the adhesion strength on a smooth

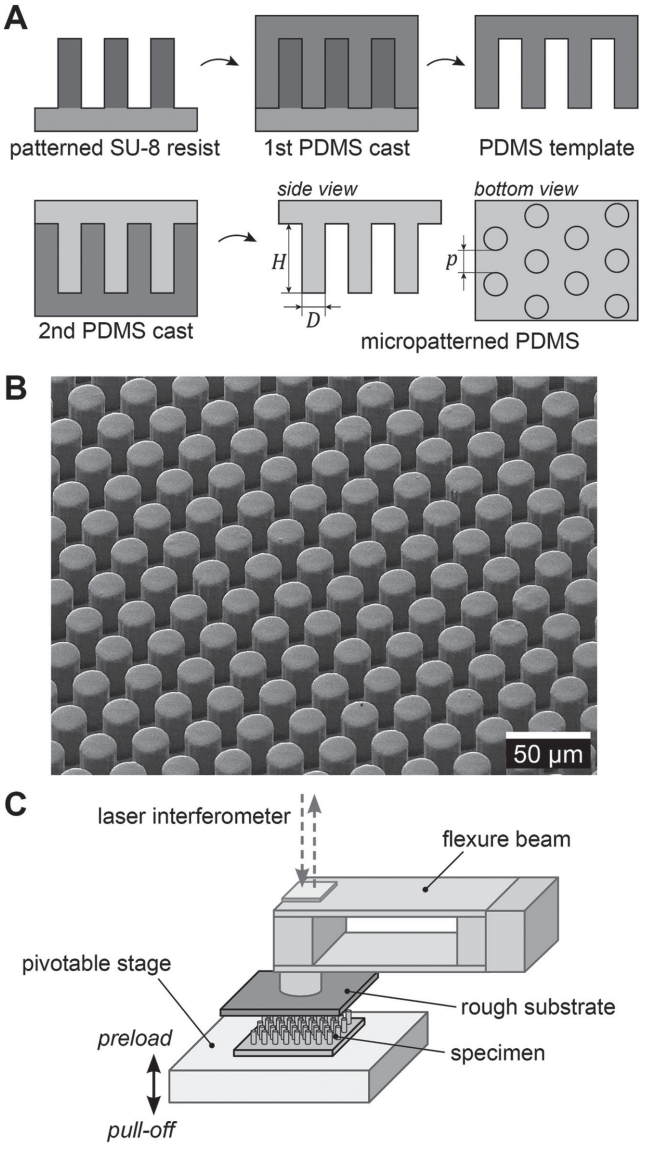

Figure 1. Process scheme for manufacturing micropatterned adhesives and experimental setup for normal adhesion measurements. A) Procedure for the fabrication of polydimethylsiloxane (PDMS) pillar array specimens using pre-patterned SU-8 templates for subsequent two-step replication into PDMS. B) Scanning electron micrograph of a representative micropatterned PDMS sample. C) Schematic illustration of the adhesion measurement device that consists of a pivotable stage for sample manipulation and a rough substrate mounted on a flexible double beam. The laser interferometer monitors the elastic deflection of the beam, from which the forces are deduced, during the measurement.

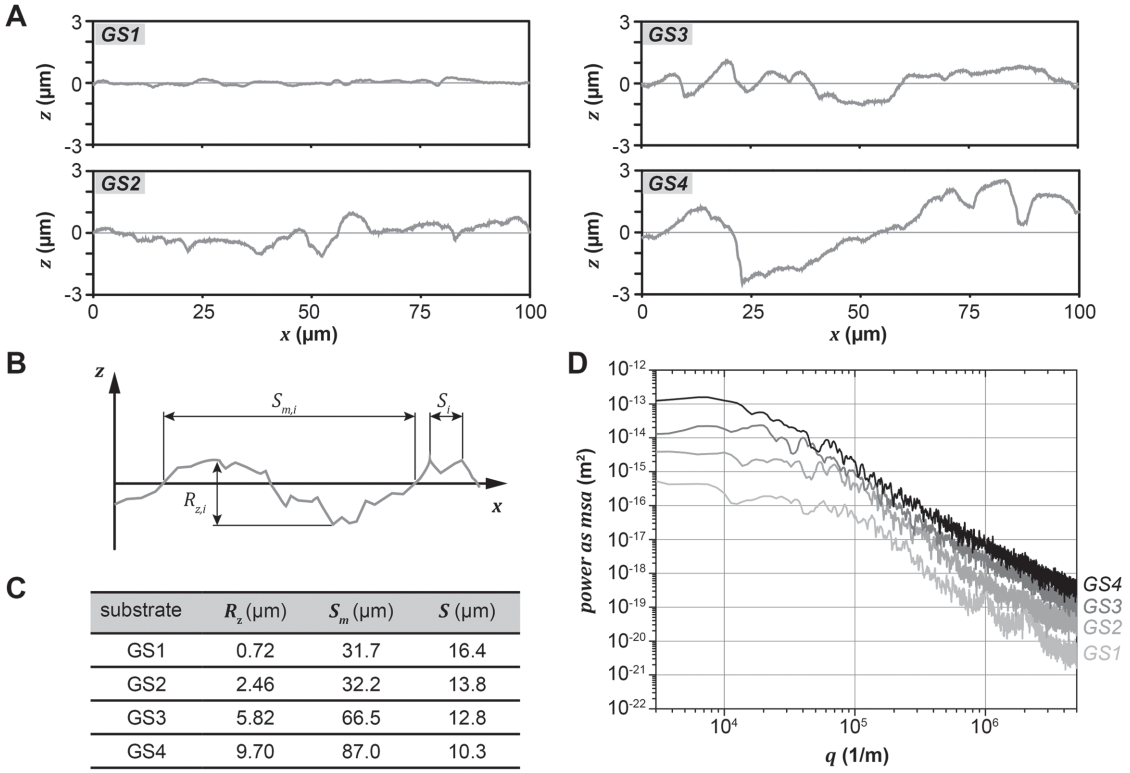

substrate	R_z (µm)	S_m (µm)	S (µm)
GS1	0.72	31.7	16.4
GS2	2.46	32.2	13.8
GS3	5.82	66.5	12.8
GS4	9.70	87.0	10.3

Figure 2. Surface topographies of rough substrates. A) Surface profiles of the roughened glass substrates GS1 to GS4 measured by profilometry. B) Schematic representation of the surface roughness parameters. The amplitude parameter of the surface profiles is the mean peak-to-valley profile roughness, given by $R_z = \frac{1}{k}\sum_{i=1}^{k} R_{z,i}$. Two spacing parameters are defined: S_m is the mean distance between successive points as they cross the mean line and is given by $S_m = \frac{1}{n}\sum_{i=1}^{n} S_{m,i}$. The mean spacing of adjacent local peaks, S, is given by $S = \frac{1}{n}\sum_{i=1}^{n} S_i$. The subscript i refers to the *i-th* location, k is the number of cut-off filter lengths, and n is the number of i measurements. C) Results of roughness mean values for the substrates GS1 to GS4 obtained from surface profilometry. D) Surface roughness power spectra of the glass substrates GS1 to GS4.

surface.[8,37] Additional data are shown in Figure 3B, where the slopes of the (logarithmic) pull-off stress values as a function of the (logarithmic) pillar diameter are indicated (Figure 3B). Accordingly, the pull-off stress (σ_c) was found to depend on the pillar diameter through a power law $\sigma_c \sim D^n$, where the exponent n is a measure of the "contact splitting efficiency."[11] On the smooth control surface, n was found to be −0.5, in agreement with earlier studies.[11,38] However, the pillar structures with diameters 30 and 50 µm and low aspect ratios were less adhesive than the fitting curve would predict. An explanation might be an elastic deformation of the backing layer in addition to the pillar deformation under preload that reduces adhesion as reported by Varenberg et al.[39] and, therefore, the smaller adhesion values of the pillars with larger diameters apparently increases the contact splitting efficiency in Figure 3A. On a rough surface, as for example GS3, a new behavior was discovered: First, two adhesive regimes were observed. Regime 1 displays a higher pull-off stress than for unpatterned PDMS (marked by the dashed horizontal line), with adhesion increasing for smaller pillar diameters. A maximum stress is attained at a critical pillar diameter of about 15 µm, below which the pull-off stress abruptly decreases to a value much smaller than for unpatterned PDMS (called regime 2). Second, the contact splitting efficiency in regime 1 is found to be $n = -0.5$ for a pillar height exceeding 20 µm, as for smooth substrates. However, the contact splitting efficiency decreased for shorter pillars, reaching a value of $n = -0.1$ for a pillar height of 5 µm. In regime 2, the contact splitting effect is virtually lost.

The pull-off stresses as a function of the pillar height are displayed in **Figure 4.** For the smooth control substrate, the measured pull-off stress was independent of pillar height (Figure 4A) and, therefore, the aspect ratio did not affect adhesion. By contrast, the pull-off stress measured on the rough substrates GS1 (Figure 4B) and GS3 (Figure 4C) strongly depended on pillar height. In regime 1 (pillar diameters exceeding 15 µm), adhesion increased with increasing pillar height, until it plateaued at a critical pillar height of about $H = 40$ µm. The pull-off stress was found to vary with H according to a power law, between $H^{0.1}$ and $H^{0.4}$. In contrast, in regime 2 (pillar diameters below 15 µm), the effect of pillar height was reversed: the pull-off stress decreased with an increase in pillar height, eventually attaining a minimum. Before the minimum, the pull-off stress varied as a function of the pillar height from $H^{-0.2}$ to $H^{-1.4}$.

Both regimes can be illustrated in contour plots (**Figure 5**) in which the values of the pull-off stress are represented as functions of pillar diameter and height. Interestingly, the locations

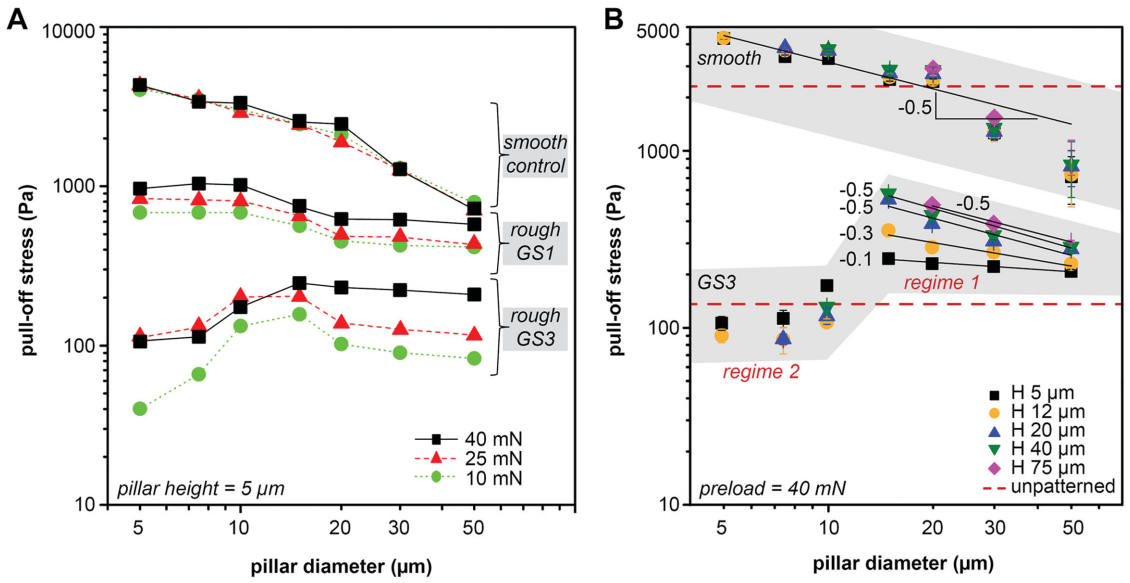

Figure 3. Results of adhesion measurements of PDMS pillar array specimens on smooth and rough substrates. A) Effects of the preload and pillar diameter on normal adhesion: Pull-off stress as a function of the pillar diameter for certain applied preloads varying from 10 to 40 mN. Measurements were performed on the rough substrates GS1 and GS3 and the smooth control. The height of the pillar structures was 5 μm. B) The effect of pillar height on pull-off stress as a function of pillar diameter at a constant preload of 40 mN. The black solid lines represent linear fits in the diameter range between 15 to 50 μm (regime 1) on the rough substrate and over the whole range of pillar diameters for the smooth substrate. The numbers −0.5 to −0.1 represent the slopes of the linear fits in the log–log plots and are referred to as the contact splitting efficiency in the text. The dashed line represents the pull-off stress of the unpatterned PDMS specimen measured on the rough substrate GS3. The gray zones are provided to guide the eye.

of the regimes vary only slightly for all rough substrates (GS1 to GS4) used in this study. Regime 2 is located within the 5 to 15 μm pillar diameter range and within the 12 to 20 μm pillar height range (GS1 and GS2) or the 5 to 20 μm pillar height range (GS3 and GS4). The remaining area displayed in the contour plot represents the adhesive regime 1, in which the adhesion increased for smaller and taller pillar structures, that is for higher aspect ratios. This finding is in line with an earlier analytical study that predicts higher adhesion of fibrillar structures with higher aspect ratio due to enhanced compliance of the micropatterned array and, therefore, better adaptation to rough substrates.[28] Interestingly, high aspect ratios are frequently found in the design of natural dry adhesives as in the case of insects and geckoes.

3. Discussion

The results presented above suggest that rough substrates introduce additional effects when they adhere to a micropatterned array of fibrils: in contrast to smooth substrates, adhesion now depends on the preload and the dimensions of the fibrils, in addition to the surface roughness itself. In this study, we have for the first time identified two different interaction regimes: in regime 1, adhesive values exceed those of the unpatterned PDMS adherent, whereas typically lower adhesive values compared to the unpatterned adherent are found in regime 2. We therefore propose to name regime 1 the "adhesive regime" and regime 2 the "non-adhesive regime."

Our observations can be qualitatively rationalized by considering the mechanisms of contact formation between an elastic pillar structure and a rigid, rough substrate. Initial contact will occur only at the local peaks on the substrate. The contact area will be immediately increased due to free surface energy minimization in accordance with the Johnson, Kendall and Roberts (JKR) theory.[40] As compressive preload is applied, the pillar structure will be forced to adapt to the surface topography of the substrate. Two mechanisms can come into play: elastic deformation predominantly in the axial direction and off-axis pillar bending or buckling. Which of these mechanisms is predominant will depend on the pillar dimensions in relation to the roughness values in the following way:

i) In the adhesive regime 1, the pillar diameter of the fibrils is always larger than the mean spacing, S, of adjacent local peaks on all rough substrates (i.e., $D > S$). In this case, the pillars will rest on several local roughness peaks; hence contact area will be increased mostly by local elastic deformation of the pillars without significant bending or buckling (**Figure 6**A). The energy stored in the required local elastic deformation will increase with the peak-to-valley distance, R_z, of the rough substrate; this strain energy penalty will, however, decrease for taller pillars. This can explain why larger R_z values lead to lower adhesion (as is known from the literature[28,32,33,35] and shown in Figures 3A, 4, and 5) while taller pillars show better adhesion (see Figures 3B and 4). In this regime, the adhesion force of fibrillar surfaces was increased by a factor between 2.7 (for GS1) and 4.2 (for GS3) over that of the unpatterned control surface.

ii) In the non-adhesive regime 2, the pillar diameter is smaller than the mean spacing of adjacent local peaks (i.e., $D < S$). Therefore, the pillar faces will now predominantly meet the substrate in the sidewalls of grooves and peaks to

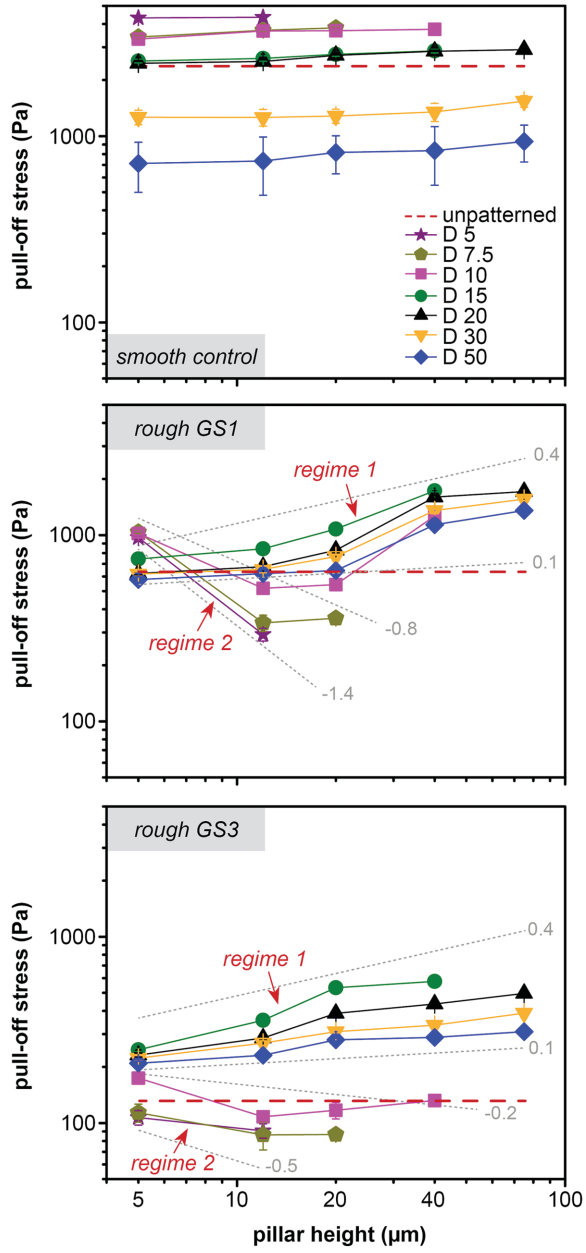

Figure 4. Effect of the pillar height of PDMS pillar array specimens on the results of normal adhesion measurements. The measurements were performed on the rough substrates GS1 and GS3 in reference to the smooth control. The pillar diameters, D, were varied from 5 to 50 μm and the applied preload was kept constant at about 40 mN. The dashed red lines represent the pull-off stress for an unpatterned PDMS specimen. The gray dotted lines represent the range of positive and negative dependence on pillar height in regimes 1 and 2, respectively. The numbers represent the slopes.

accommodate the local misorientation. Now, bending of the pillars will be more efficient for achieving a larger contact area as demonstrated in Figure 6B. The off-axial bending of the pillars results in elastic bending energy that in addition to the elastic strain energy by local elastic deformation at the pillar faces (see regime 1) works against the adhesive energy. We argue that the higher elastic energy resulting from this process can explain the lower adhesion forces measured in this regime. The bending energy shows a strong size dependence: a pillar diameter dependence of $\sim D^4$ and a pillar height dependence of $\sim H^{-2}$. For arbitrarily small pillar structures, the bending energy of the total array is, therefore, expected to vanish. Hence, we cannot exclude the possibility that adhesion values will increase again for much smaller pillars (<5 μm in diameter) than studied in this paper. Such small dimensions would be reminiscent of the length scale of adhesion organs of large animals such as geckoes, which exhibit terminal elements on the nanoscale.

Another phenomenon that will reduce adhesion to rough surfaces is the increased propensity for buckling on rough surfaces with a resulting loss of contact between pillar and substrate.[41] When a perfectly aligned array of micropillars comes into contact with a smooth surface, all pillars contact the substrate fully in one step, without buckling (provided that the preload is smaller than the critical buckling load). On the other hand, the same array will only gradually come into contact with a rough substrate due to the height irregularities. The pillars that do come into contact with the surface will carry the entire load and will be more likely to buckle. As the critical load for buckling varies with the number of pillars in contact with the substrate, the pillars that formed contact early on will also tend to buckle first and will not be able to contribute much to adhesion under tension. Note that buckling will more likely occur for aspect ratios larger than 1. However, the propensity for buckling is enhanced by the axial noneccentric loading due to local misorientation of the pillar faces to the surface asperities. We argue that this explains the lowest adhesion values in regime 2 obtained for pillar heights of 12 and 20 μm, in contrast to slightly better adhesion for only 5 μm tall pillar structures (see Figure 4).

Overall, our results suggest a new strategy for optimizing fibrillar surfaces in contact with rough surfaces. The most relevant finding in light of possible applications is that fibrillar adhesive microstructures do not increase adhesion only to smooth surfaces, according to the principle of contact splitting, as has been reported frequently. Also for rough substrates, fibrillar structures demonstrated increased adhesion, provided that the fibril diameter is chosen judiciously with regard to the substrate roughness: D must lie close to, but above the lateral roughness parameter S of the substrate (to avoid bending and buckling). In addition, a large pillar height should be chosen (to minimize elastic strain energy). In any case, the transition region between the adhesive regime 1 and the non-adhesive regime 2 as defined in our paper must be avoided.

4. Conclusions

We present a detailed study of normal adhesion for micropatterned adhesives on rough, rigid substrates. For the first time, a systematic variation of pillar diameters and heights was performed and the adhesion force values were analyzed in connection with the roughness parameters of the substrate. The following conclusions were drawn:

i) Fibrillar adhesive surfaces can improve the adhesion to rough substrates by a factor between 2 and 4 compared to

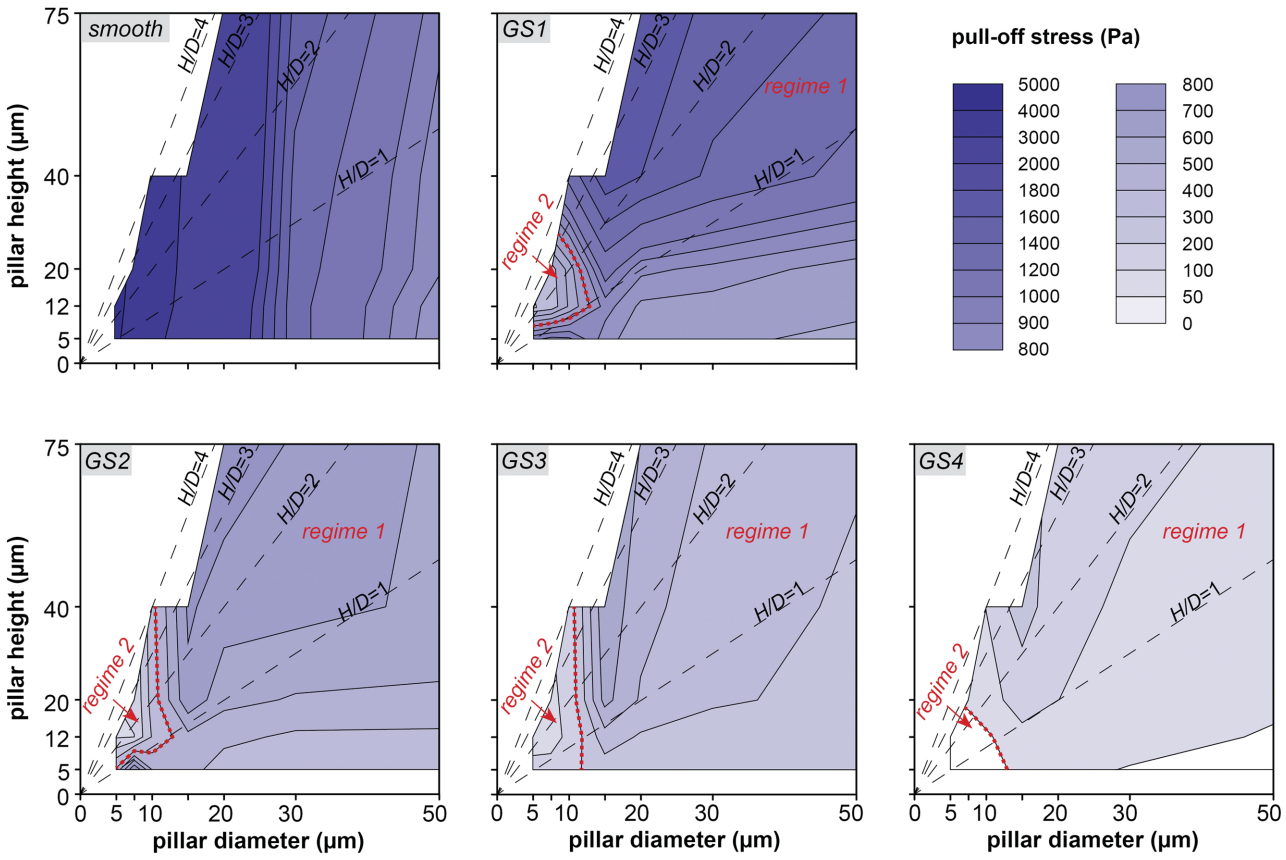

Figure 5. Adhesion as a function of pillar diameter and height: The contour plots represents the pull-off stress values as a function of pillar height and pillar diameter for all rough substrates GS1 to GS4 in reference to the smooth control. The colors correspond to different pull-off stress values. The black dashed lines represent the aspect ratios (H/D) of the pillars. The red dashed lines represent the transition from the adhesive regime 1 to the nonadhesive regime 2.

unpatterned surfaces. The principle of "contact splitting," advocated first for smooth substrates, has thus been shown to apply also to rough substrates.

ii) To take advantage of this effect, the dimensions of the fibrils must be chosen in relation to the roughness parameters of the substrate. The fibril diameter should be small, but not

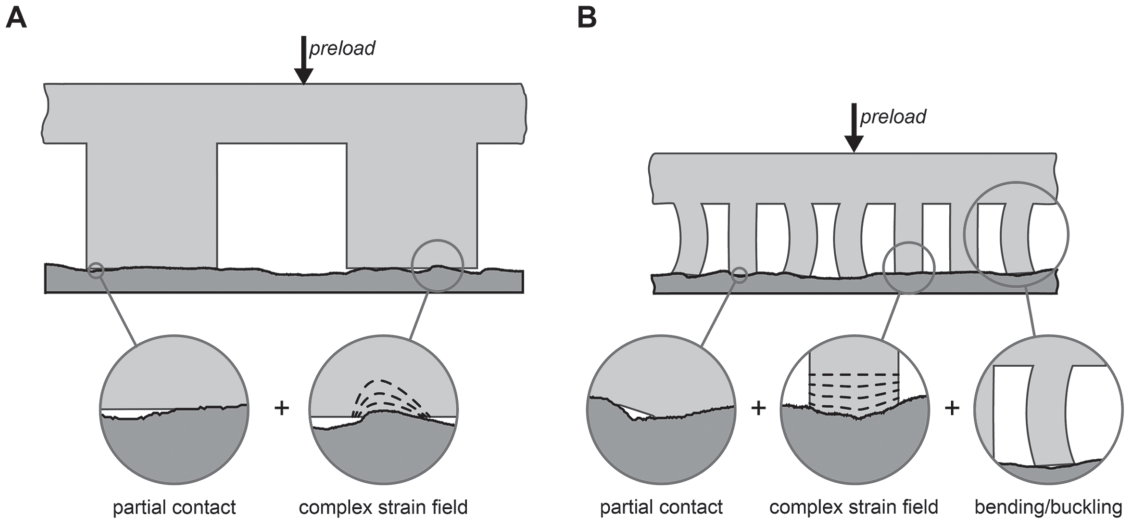

Figure 6. Contact mechanisms for regimes 1 and 2: Schematic illustration of a micropatterned array of pillars pressed onto a rough substrate in A) regime 1 and B) regime 2. Insets represent the partial contact and a complex strain field at the pillar faces found to occur in both regimes. Additionally, bending and buckling of pillars can occur in regime 2 as shown in the inset.

smaller than the mean spacing between local peaks on the substrate. The pillar height should be as large as possible without jeopardizing stability.

iii) Two new regimes of adhesion were identified: regime 1, in which the diameter of pillars exceeds the spacing between the local peaks of the substrate, and regime 2 where the converse relationship applies. The superior adhesion in regime 1 was attributed to only small elastic deformations required in forming contact; by contrast, the nonadhesive regime 2 is ascribed to frequent pillar bending and buckling events, which store much energy and reduce the contact area.

iv) Contour plots were developed, which depict the coexistence of both regimes as a function of both pillar diameter and height. This makes the adhesion of micropillar arrays on rough substrates distinct from that on a smooth substrate. We believe that these results are particularly relevant for designing micropatterned adhesives suitable for both adhesive and nonadhesive phenomena and applications connected to surface roughness.

5. Experimental Section

Sample Fabrication: Fibrillar gecko-mimetic adhesives were fabricated by soft molding PDMS (Dow Corning, Sylgard 184 kit) from master templates (see Figure 1A). Master templates were fabricated from silicon wafers spin coated with a negative photoresist, SU-8 (Micro Resist Technology, Berlin, Germany), using a standard photolithography process. The mask employed during the UV exposure step of the photolithography process consisted of 25 fields of hexagonally packed circles of different diameters and spacings. Prior to soft molding, templates were silanized by exposure to approximately 50 µL of hexadecafluoro-1,1,2,2-tetrahydrooctyltrichlorosilane (Alfa Aesar, Germany) under vacuum for 30 min. The templates were then placed in an oven at 95 °C for 30 min. The PDMS base and crosslinker were mixed (10:1 ratio) and degassed in a desiccator to eliminate bubbles. This mixture was poured onto the templates, degassed again, and cured at 75 °C for 24 h to produce the PDMS micropatterned samples. These samples were then carefully peeled off the templates. Each resulting PDMS micropatterned sample consisted of 25 8×8 mm$^{[2]}$ regions each with different pillar heights (5, 12, 20, 40, or 75 µm) and diameters (5, 7.5, 10, 15, 20, 30, or 50 µm). The PDMS fibrillar arrays of different pillar heights, diameters, and aspect ratios were characterized using a scanning electron microscope (SEM) (FEI Quanta 400 ESEM) operating under high vacuum and with a beam energy of 1–15 kV.

Preparation and Characterization of Rough Surfaces: Flat glass was selected as the substrate of choice to study the adhesion of the PDMS fibrillar samples. Each substrate was roughened with sandpaper (Buehler GmbH, Düsseldorf, Germany) of different asperity sizes. These rough substrates were in turn used as substrates for adhesion measurements. The roughness profile of each substrate was determined using a profilometer (Surform 1500 SD3, Zeiss GmbH) (Figure 2A). Measurements were made using a 1 µm radius stylus at 0.3 mm s^{-1} scan speed. Three measurements were taken at different locations on each sample.

The amplitude parameter is the mean peak-to-valley profile roughness that is given by $R_z = \frac{1}{k}\sum_{i=1}^{k} R_{z,i}$, where k is the number of cut-off filter lengths and z_i is the peak to valley distance at the *i-th* location. Two spacing parameters are defined as follows: S_m is the mean distance between successive points as they cross the mean line and is given by $S_m = \frac{1}{n}\sum_{i=1}^{n} S_{m,i}$. The mean spacing of adjacent local peaks, S, is given by $S = \frac{1}{n}\sum_{i=1}^{n} S_i$. The power spectra of the glass substrates GS1 to GS4 were calculated based on the amplitude of the Fourier transformed data from the line scans using Origin, (*OriginLab, v. 9*). Normalization of the power spectrum was performed via the mean square amplitude (MSA) method, i.e., $\frac{Re^2 + Im^2}{n^2}$ where *Re* and *Im* are the real and imaginary parts of the transform data and n is the length of the input sequence.

Adhesion Measurements: Normal adhesion was measured using a custom-built adhesion-measuring device (Figure 1C).[31,42] The base of the device consists of a three-axis piezo stage (Nanocube, physics instruments Karlsruhe, Germany), with nanoscale resolution, sitting on a pivotable six-axis table (Hexapod F.206, physics instruments Karlsruhe, Germany), which is adjustable on the microscale in the x, y, and z directions, for sample positioning. Adhesion to a sample on the stage was measured using a force sensor system comprised of a glass spring (with a spring constant of 2450.7 N m^{-1}) and a laser interferometer. The spring consists of an asymmetrically strained glass slide onto which a mirror is mounted to reflect the light from the laser (SP 100, SIOS Messtechnik, Ilmenau, Germany). The substrate, against which the samples adhesion is tested, was glued onto an adapter with cyanoacrylate glue (Cyanolube, HK Wentworth Ltd., Derbyshire). To allow for further adjustment of the position of the glass spring, the spring is mounted onto a two-axis tilt stage (OWIS GmbH, Stauffenberg, Germany). The whole device sits on an anti-vibration tabl e (TS 150, Technical Manufacturing Corporation, USA) to reduce the noise arising during measurements.

For adhesion measurements, the desired PDMS sample was placed on the pivotable stage and the substrate was immobilized on the spring. The substrate was manually aligned with the sample, such that the surfaces of each were parallel to each other, using two cameras, one located on the y-axis and the other on the x-axis of the sample. Alignment was further optimized by mechanically adjusting the sample stage along the x- and y-axes until a maximum pull-off force was achieved for a constant preload. Once the optimal sample position was identified, the sample was cleaned with ethanol and the pull-off force was measured for each rough surface. Each data point represents the mean value of five measurements on four different in-plane positions on each substrate. The error bars indicate the standard deviation. The adhesion of flat, unpatterned PDMS samples, in addition to the micropatterned PDMS samples, was characterized for control purposes. All measurements were performed at an approach/retraction velocity of 5 µm s^{-1} at a controlled temperature and relative humidity (RH) of 24 °C and 40% RH, respectively. The adhesion results are presented as pull-off stress values, which were derived by dividing the measured force by the apparent contact area.

Acknowledgements

V.B., N.K.G., and E.A. contributed with conception and experimental design. V.B. performed the experiments. V.B., R.H., A.G., and R.M.M. carried out analysis and interpretation of data. V.B., R.H., A.G., and E.A. wrote the manuscript. V.B. and R.H. contributed equally to this work. V.B. acknowledges funding by SPP 1420 of the German Science Foundation DFG. E.A., N.K.G., and R.H. acknowledge funding from the European Research Council under the European Union/ERC Advanced Grant "Switch2Stick," Agreement No. 340929.

Received: February 4, 2016
Revised: March 14, 2016
Published online: May 9, 2016

[1] K. Autumn, M. Sitti, Y. A. Liang, A. M. Peattie, W. R. Hansen, S. Sponberg, T. W. Kenny, R. Fearing, J. N. Israelachvili, R. J. Full, *Proc. Natl. Acad. Sci. USA* **2002**, *99*, 12252.
[2] K. Autumn, A. M. Peattie, *Integr. Comp. Biol.* **2002**, *42*, 1081.
[3] E. Kroner, C. S. A Davis, *J. Adhes.* **2015**, *91*, 481.

[4] G. Huber, H. Mantz, R. Spolenak, K. Mecke, K. Jacobs, S. N. Gorb, E. Arzt, *Proc. Natl. Acad. Sci. USA* **2005**, *102*, 16293.
[5] T. W. Kim, B. Bhushan, *J. R. Soc., Interface* **2008**, *5*, 319.
[6] K. Autumn, Y. A. Liang, S. T. Hsieh, W. Zesch, W. P. Chan, T. W. Kenny, R. Fearing, R. J. Full, *Nature* **2000**, *405*, 681.
[7] Y. Tian, N. Pesika, H. Zeng, K. Rosenberg, B. Zhao, P. McGuiggan, K. Autumn, J. Israelachvili, *Proc. Natl. Acad. Sci. USA* **2006**, *103*, 19320.
[8] E. Arzt, S. Gorb, R. Spolenak, *Proc. Natl. Acad. Sci. USA* **2003**, *100*, 10603.
[9] S. N. Gorb, *Functional Surfaces in Biology*, Vol. *2*, Springer, Heidelberg, Germany, **2009**.
[10] H. Gao, X. Wang, H. Yao, S. Gorb, E. Arzt, *Mech. Mater.* **2005**, *37*, 275.
[11] R. Spolenak, S. Gorb, H. Gao, E. Arzt, *Proc. R. Soc. A: Math. Phys. Eng. Sci.* **2005**, *461*, 305.
[12] Y. Mengüç, M. Sitti, *Polymer Adhesion, Friction, and Lubrication*, Vol. *10*, John Wiley & Sons, Inc, Hoboken, NJ., **2013**, pp. 351–389, DOI: 10.1002/9781118505175.ch9.
[13] L. Heepe, S. N. Gorb, *Annu. Rev. Mater. Res.* **2014**, *44*, 173.
[14] A. Jagota, C. Y. Hui, *Mater. Sci. Eng. R: Rep.* **2011**, *72*, 253.
[15] A. Pattantyus-Abraham, J. Krahn, C. Menon, *Front Bioeng. Biotechnol.* **2013**, *1*, 1.
[16] M. Zhou, N. Pesika, H. Zeng, Y. Tian, *Friction* **2013**, *1*, 114.
[17] M. Kamperman, E. Kroner, A. Del Campo, R. M. McMeeking, E. Arzt, *Adv. Eng. Mater.* **2010**, *12*, 335.
[18] C. Greiner, in *Biomimetic and Bioinspired Nanomaterials*, Vol. *7*, (Ed.: C. S. S. R: Kumar), Wiley-VCH, Weinheim, Germany, **2010**, pp. 1–39.
[19] L. F. Boesel, C. Greiner, E. Arzt, A. del Campo, *Adv. Mater.* **2010**, *22*, 2125.
[20] G. Huber, S. N. Gorb, N. Hosoda, R. Spolenak, E. Arzt, *Acta Biomater.* **2007**, *3*, 607.
[21] A. G. Gillies, A. Henry, H. Lin, A. Ren, K. Shiuan, R. S. Fearing, R. J. Full, *J. Exp. Biol.* **2014**, *217*, 283.
[22] B. N. J. Persson, *MRS Bull.* **2007**, 32, *486*.
[23] B. N. J. Persson, *J. Chem. Phys.* **2003**, *118*, 7614.
[24] J. Davies, S. Haq, T. Hawke, J. P. Sargent, *Int. J. Adhes. Adhes.* **2009**, *29*, 380.
[25] A. Asbeck, S. Dastor, A. Parness, L. Fullerton, N. Esparza, D. Soto, B. Heyneman M. Cutkosky, in *Proc. IEEE Int. Conf. on Robotics and Automation*, IEEE, Kobe, Japan, Vol. *10*, **2009**, p. 2675.
[26] S. Vajpayee, A. Jagota, C.-Y. Hui, *J. Adhes.* **2010**, *86*, 39.
[27] N. Cañas, M. Kamperman, B. Völker, E. Kroner, R. M. McMeeking, E. Arzt, *Acta Biomater.* **2012**, *8*, 282.
[28] C.-Y. Hui, N. J. Glassmaker, A. Jagota, *J. Adhes.* **2005**, *81*, 699.
[29] H. Kasem, M. Varenberg, *J. R. Soc., Interface* **2013**, *10*, 20130620.
[30] C. T. Bauer, E. Kroner, N. A. Fleck, E. Arzt, *Bioinspiration Biomimetics* **2015**, *10*, 66002.
[31] E. Kroner, R. Maboudian, E. Arzt, *Adv. Eng. Mater.* **2010**, *12*, 398.
[32] B. N. J. Persson, O. Albohr, U. Tartaglino, A. I. Volokitin, E. Tosatti, *J. Phys. Condens. Matter* **2005**, *17*, R1.
[33] K. N. G. Fuller, D. Tabor, *Proc. R. Soc. Lond. A: Math. Phys. Sci.* **1975**, *345*, 327.
[34] G. A. D. Briggs, B. J. Briscoe, *J. Phys. D: Appl. Phys.* **1977**, *10*, 2453.
[35] B. N. J. Persson, E. Tosatti, *J. Chem. Phys.* **2001**, *115*, 5597.
[36] E. Kroner, D. R. Paretkar, R. M. McMeeking, E. Arzt, *J. Adhes.* **2001**, *87*, 447.
[37] C. Greiner, A. Del Campo, E. Arzt, *Langmuir* **2007**, *23*, 3495.
[38] A. Del Campo, C. Greiner, E. Arzt, *Langmuir* **2007**, *23*, 10235.
[39] M. Varenberg, B. Murarash, Y. Kligerman, S. N. Gorb, *Appl. Phys. A: Mater. Sci. Process.* **2011**, *103*, 933.
[40] K. L. Johnson, K. Kendall, A. D. Roberts, *Proc. R. Soc. A: Math. Phys. Eng. Sci.* **1971**, *324*, 301.
[41] D. R. Paretkar, M. D. Bartlett, R. McMeeking, A. J. Crosby, E. Arzt, *J. Adhes.* **2013**, *89*, 140.
[42] E. Kroner, J. Blau, E. Arzt, *Rev. Sci. Instrum.* **2012**, *83*, 016101.